☙

Photoneutralization and slow capture of carriers in quantum dots probed by resonant excitation spectroscopy

Hai Son Nguyen,[1,*] Gregory Sallen,[1,†] Marco Abbarchi,[1,‡] Robson Ferreira,[1] Christophe Voisin,[1] Philippe Roussignol,[1] Guillaume Cassabois,[1,2,3] and Carole Diederichs[1,§]

[1]*Laboratoire Pierre Aigrain, Ecole Normale Supérieure, CNRS (UMR8551), Université P. et M. Curie, Université D. Diderot, 24 rue Lhomond, F-75231 Paris Cedex 05, France*
[2]*Université Montpellier 2, Laboratoire Charles Coulomb (UMR5221), F-34095 Montpellier, France*
[3]*CNRS, Laboratoire Charles Coulomb (UMR5221), F-34095 Montpellier, France*

We investigate experimentally and theoretically the resonant emission of single InAs/GaAs quantum dots in a planar microcavity. Due to the presence of at least one residual charge in the quantum dots, the resonant excitation of the neutral exciton is blocked. The influence of the residual doping on the initial quantum dots charge state is analyzed, and the resonant emission quenching is interpreted as a Coulomb blockade effect. The use of an additional nonresonant laser in a specific low power regime leads to the quantum dots neutralization and allows an efficient optical gating of the exciton resonant emission. A detailed population evolution model, developed to describe the quantum dot neutralization and the optical gate effect, perfectly fits the experimental results in the steady-state and dynamical regimes of the optical gate with a single set of parameters. We deduce that ultraslow Auger- and phonon-assisted capture processes govern the quantum dot neutralization with relaxation times in the 1–100 μs range. We conclude that the optical gate acts as a very sensitive probe of the quantum dots population relaxation in an unprecedented slow-capture regime.

PACS number(s): 78.67.Hc

I. INTRODUCTION

Most of the spectroscopic experiments in single quantum dots (QDs) are performed under nonresonant excitation. In such a configuration, the nonresonant laser creates carriers in the barrier or in the wetting layer. The photocreated carriers then relax to the QD excited states via *capture* of the carriers from the barrier or the wetting layer to the confined QD excited states. Then, *intradot relaxation* processes between the different QD discrete states lead to electron and hole population of the ground states from which the QD photoluminescence occurs. Theoretical works show that the capture mechanism relies either on emission of optical phonons[1,2] with typical capture times between 100 fs and 100 ns, or on electron-electron and electron-hole Auger scattering[3,4] with typical capture times between 1 ps and 1 μs. These calculations are in perfect agreement with time-resolved experiments performed in QDs ensemble[5] and in single QDs[6] where capture times of the order of 100 ps have been measured. On the other hand, irreversible Auger scattering is mainly responsible for the intradot relaxation process, and theoretical calculations[1,7] give estimate of the corresponding relaxation times in the 100-fs to 10-ps range. In fact, differential transmission measurements,[8] pump-probe spectroscopy,[9] and time-resolved experiments[10,11] showed that the Auger-assisted processes involved in the intradot carriers relaxation occur within characteristic times between 1 ps and 10 ps. In total, theoretical and experimental results show that the intradot relaxation times are generally much shorter (from 100 fs to 10 ps) than the characteristic times of the carriers capture from the continuum (up to 1 μs). The relaxation times to the QD ground states are thus often only attributed to the capture time. Nevertheless, intradot relaxation processes, although secondary in the population relaxation, play a very important role in the coherence relaxation.[12,13]

The QD coherence is another fundamental aspect that has been widely studied. At low temperature, the QD coherence is limited by spontaneous emission and QD coupling to its fluctuating environment. When spontaneous emission is the only dephasing process, the QD coherence is in the so-called radiative limit and in this ideal case, QDs appear as ideal systems to transpose the atomic physics concepts to the solid state. In this context, major experimental results have been obtained in single QDs, such as the emission of single[14] and indistinguishable[15] photons, the Rabi oscillations,[16] and the strong coupling regime between a single QD and an optical microcavity.[17,18] However, the radiative limit is hardly reached, showing that the intuitive artificial atom picture is strongly influenced by the QD environment.

As previously shown by Kammerer *et al.*,[19] strictly resonant excitation of single QDs is a crucial requirement in order to minimize the dephasing processes induced by the phonon and Auger-assisted carriers capture. Since the first direct measurement of the optical response of single QDs under resonant excitation performed by Muller *et al.*,[20] many results on resonant emission (RE) in single QDs were presented in the literature.[21–25] However, except for studies in the RE low power regime where the coherence is driven by the resonant excitation laser,[26–28] the radiative limit is never reached even at very low temperature. This suggests that a fluctuating electrostatic environment which influences the QD coherence still exists, even in the case of resonant excitation where the laser photocreated carriers are only in the QD. Our recent work on the quenching of the QD RE strongly corroborates this assumption.[24] The resonant excitation of the neutral exciton in single QDs can be completely inhibited by a Coulomb blockade effect because of the presence of at least one residual charge in the QD. However, this issue is overcome with the use of an additional weak nonresonant laser which neutralizes

the QD and optically gates its RE,[24] as also shown in other recent experimental studies.[25,28,29] The use of an additional weak nonresonant laser also appears to be interesting to probe the local environment fluctuations at the single-charge level in single QD[30] and to minimize these environment fluctuations to improve the emitted photons indistinguishability.[31]

The present paper is devoted to a comprehensive experimental and theoretical study of this optical gating effect in single QDs under resonant excitation. The influence of the residual doping on the initial QD charge state, and consequently on the QD RE quenching, is analyzed. Moreover, a detailed population evolution model is developed to describe the QD neutralization by the weak optical gate. This model which perfectly fits, with a single set of parameters, the experimental results in the steady-state and dynamical regimes, shows that the QD neutralization is governed by peculiar Auger- and phonon-assisted capture processes. In fact, beyond the explanation of the optical gate effect, the original weak optical gate configuration allows us to study an unprecedented regime where the carriers capture involved in the QD neutralization is governed by ultraslow processes with time constants of the order of 1–100 μs. Therefore, the optical gate appears to be a very sensitive probe of the residual doping of the sample and of the QD population in a regime of a very weak nonresonant excitation.

The paper is organized as follows: In Sec. II, we give some details on the sample and the experimental configuration. Section III is devoted to the resonant excitation results on a single QD, showing a striking quenching of the neutral exciton RE which appears to be a general behavior. When such a situation is observed, the use of an additional nonresonant laser that acts as an optical gate allows a complete retrieval of the neutral exciton RE. In parallel in the Appendix, we develop a self-consistent calculation of the influence of the residual doping on the QD charge state in the absence of optical excitation. The calculations show that the RE quenching can be interpreted as a Coulomb blockade effect where at least one residual charge in the QD blocks the resonant excitation of the neutral exciton. The optical gate phenomenology is then presented in an experimental study of the RE intensity and energy shift as a function of the optical gate power. Section IV presents a population evolution model where the different carriers capture and escape processes induced by the optical gate are considered. Section V is finally devoted to a confrontation of our theoretical model to experimental data on the optically gated RE obtained either in the steady-state or dynamical regime. Distinct experiments allow one to obtain a highly constrained set of parameters used in our model. Finally, as an illustration of the robustness of our approach, we reproduce quantitatively measurements of the emitted photon statistics. This statistics shows the usual antibunching at zero delay, but a strong photons bunching at larger delays. This bunching is essentially due to fluctuations of the QD between a neutral and a charged state.

II. SAMPLE DESCRIPTION AND EXPERIMENTAL SETUP

Our sample is made of a single layer of self-assembled InAs/GaAs QDs inserted in an AlAs/AlGaAs planar microcavity. The QD density varies from 10^7 to 10^{10} QDs/cm^2 with an

energy distribution of the emission from 1.240 eV to 1.305 eV with a maximum at 1.270 eV. In the experiments, we focus on the low density region of the sample where the QD density is about 10^8 QDs/cm^2. The planar microcavity is a Fabry-Perot cavity made of two Bragg mirrors which are composed of alternating AlAs and AlGaAs layers of identical optical thicknesses $\lambda_0/4$ ($\lambda_0 = 1$ μm). The cavity spacer is a λ_0-GaAs layer and the top and bottom Bragg mirrors are, respectively, composed of 11 and 24 AlAs/AlGaAs pairs, resulting in a quality factor of 2500. The Fabry-Perot cavity mode is then centered at 1.270 eV with a full width at half maximum of 0.55 meV. The cavity asymmetry facilitates the extraction of the QD emission in the cavity mode in our conventional confocal micro-photoluminescence setup which is used in a reflection configuration for the sample characterization under nonresonant excitation. The microscope objective used in this setup has a numerical aperture NA = 0.35 leading to a spatial resolution of 2 μm required for experimental studies on single QDs. The resonant excitation of single QDs is performed at 7 K by spatially decoupling the excitation from the detection paths in order to get rid of the elastic laser scattering.[24,26] The excitation of the QDs is done along the lateral facet of the sample by using a lensed fiber inserted in the cryostat while the detection is performed in the vertical direction with the confocal setup. The sample is fixed on a piezo-electric stage in order to optimize its position with respect to the lensed fiber. Once coupled into the sample, the laser is confined in the microcavity and propagates. The planar microcavity thus acts as a two-dimensional waveguide for the excitation laser and the main contributions to the laser scattering arise from the edge of the sample or the defects in the Bragg mirrors. Since the results presented in this paper concern the RE of a QD located far away from the edge of the sample, approximately at 1 mm, the detection of the QD emission is not disturbed by the laser scattering on the edge of the sample. In fact, as we will see in the experimental results, the laser scattering is much weaker, even negligible, than the QD signal emission. The resonant excitation laser is a cw external cavity laser diode tunable from 1.25 to 1.29 eV (i.e., from 960 to 990 nm) with a spectral resolution of 0.5 μeV and with a spectral linewidth of 1.25 neV (i.e., 300 kHz).

III. PHENOMENOLOGY OF THE OPTICAL GATE EFFECT

A. Quantum dot emission under nonresonant excitation

Under nonresonant excitation in the GaAs barrier (with a He-Ne laser), the photoluminescence spectra exhibit two distinct lines typically spaced by 1.5 meV. Figure 1(a) shows a typical nonresonant photoluminescence spectrum for a 10-μW excitation (the excitation power is measured before the microscope objective). Power-dependent studies and photon-correlation measurements[24] were performed to identify the two lines as a neutral exciton X, at the energy $E_X = 1.2736$ eV, and a charged exciton at the energy $E_{X^+} = 1.2752$ eV. Moreover, the photoluminescence of the GaAs barrier (not shown here) shows an emission line at 1.495 eV resulting from the radiative recombination of the free electrons in the barrier with the holes bound to the carbon acceptors that are the unintentional impurities which appear during the sample growth.[32] These
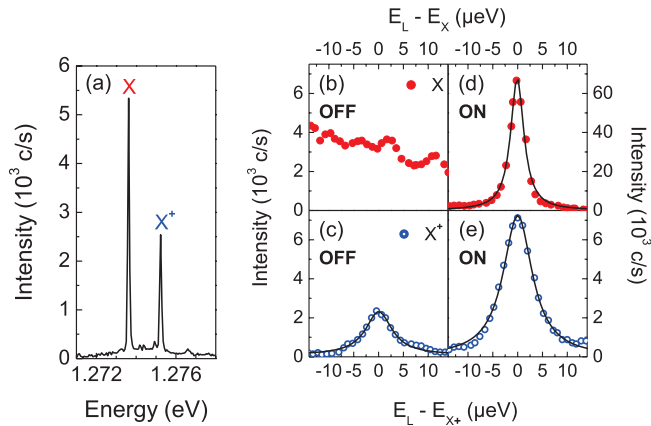
FIG. 1. (Color online) (a) Typical spectrum of the nonresonantly excited photoluminescence of a single quantum dot, showing the neutral exciton X and the positive trion X^+. (b)–(e) Resonant emission spectra of X (●) and X^+ (○) as a function of the detuning between the laser energy E_L and the exciton (trion) energy E_X (E_{X+}) when the optical gate is switched off, (b) and (c), and on, (d) and (e).

impurities are notably responsible for the presence of residual holes in the sample. Thus we consider that the charged exciton is a positive trion X^+, which is further supported by the positive detuning of the charged exciton state with respect to the neutral one.[33,34] The observation of the positive trion in the nonresonant photoluminescence spectra shows that the QDs in the studied sample may efficiently capture residual holes that exist in the QD environment. Nevertheless, under these excitation conditions, the simultaneous observation of the two lines indicates that the QD is either empty or populated by at least one hole. The situation is completely different under strictly resonant excitation.

B. Quenching of the neutral exciton resonant emission

In fact, we have recently reported on the quenching of the resonant emission of single QDs at the energy of the neutral exciton.[24] As shown in Fig. 1(b) where the RE is plotted as a function of the laser detuning with respect to the neutral exciton energy, no resonance is observed at zero detuning whereas the corresponding experiment for the positive trion shows clearly a signal enhancement when the laser energy perfectly matches its energy [Fig. 1(c)]. A statistical study showed that for more than 90% of the QDs, the RE signal arises only from the positive trion. This is due to the presence of at least one residual hole in the QDs. These residual charges induce a photon absorption at the energy of charged excitonic complexes and not at the neutral exciton one for which the QD must be empty. This phenomenon is similar to the Coulomb blockade effect where the creation of a neutral exciton is blocked by the residual hole in the QD.[24] This difficulty can be circumvented by the use of a very weak additional nonresonant laser (optical gate).

C. Control of the resonant emission by an optical gate

Starting from the experimental configuration used for the QD resonant spectroscopy (see Sec. II), an additional laser (He-Ne laser) is injected perpendicularly to the sample surface
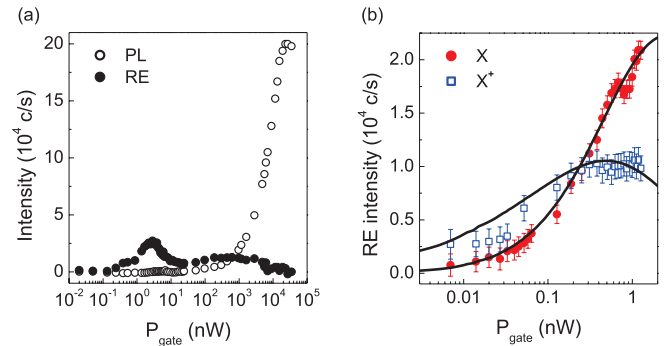
FIG. 2. (Color online) (a) Resonant emission (RE) and non-resonant photoluminescence (PL) intensities of the neutral exciton (X) as a function of the optical gate power P_{gate}. (b) Resonant emission intensity of the neutral exciton (X) and the positive trion (X^+) as a function of the optical gate power P_{gate}. Only the region where the nonresonant photoluminescence is completely negligible is displayed. The experimental data are fitted by the population evolution model described in Sec. IV (solid lines).

via the confocal microscopy setup. This additional laser acts as an optical gate for the QD RE.[24,25,28,29] Because of the very low gate power [$P_{gate} \sim 3$ nW in Figs. 1(d) and 1(e)], the nonresonant laser does not populate significantly the QD. Power-dependent studies [presented in Sec. III D, Fig. 2(a)] show indeed that the photoluminescence induced by the HeNe laser cannot be distinguished from the noise background for a typical excitation power smaller than 0.1 μW. Optical gating of the QD RE of the neutral exciton and the positive trion are presented in Figs. 1(d) and 1(e). A strong RE signal is now detected for the neutral exciton with an enhancement factor of about 30. These data show that an ultraweak nonresonant laser tends to neutralize the QD and then allows the resonant excitation of the neutral exciton. This optical gate also acts on the trion with an enhancement factor of 3. As a consequence, we assume that the QD contains possibly more than one hole when the gate is off. This assumption is supported by the self-consistent calculation of the QD population presented in the Appendix.

D. Resonant emission intensity versus the optical gate power

Figure 2(a) presents the intensity of the optically gated RE and the nonresonant photoluminescence of the exciton as a function of the optical gate power over seven orders of magnitude. The photoluminescence signal, which starts to be significant at $P_{gate} \sim 0.1$ μW, shows a standard power dependence with a saturation at $P_{gate} \sim 30$ μW. Concerning the optically gated RE, measured for a constant resonant excitation power of 5 μW (the saturation regime appears for a resonant excitation power of 16.5 μW[24]), three remarkable features can be distinguished. First, the RE appears at $P_{gate} \sim$ 0.1 nW and increases to a maximum value $I_{max} \sim 3.10^4$ counts/s for $P_{gate} \sim 3$ nW while in this region the nonresonant photoluminescence remains below the detection threshold. Once the maximum signal is reached, the optically gated RE rapidly decreases for gate powers ranging between 3 and 30 nW. At this latter excitation power, the intensity of nonresonant photoluminescence starts to be detectable. From
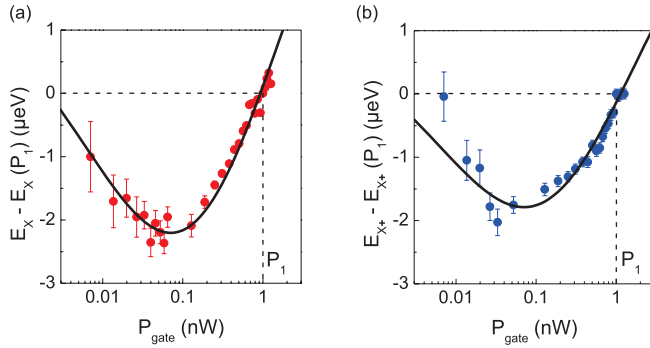
FIG. 3. (Color online) Energy of the neutral exciton (a) and positive trion (b) resonant emission as a function of the optical gate power P_{gate}. The experimental data are obtained from the same set of measurements as Fig. 2(b) and are fitted by the model described in Sec. IV (solid lines).

FIG. 4. (Color online) (a) Scheme of a QD with a fundamental hole state S_h quasiresonant with a slightly confined interfacial defect state Φ. The QD is filled with two holes and the absorption of a photon at the neutral exciton energy is impossible. (b) The capture and escape processes are schematized with the corresponding rates in a diagram showing the intrinsic hole reservoir induced by the residual doping of the sample (see Appendix), the defect, and the QD.

0.1 μW, the photoluminescence excited by the optical gate becomes significant while the RE decreases and becomes negligible at $P_{\text{gate}} \sim 30$ μW where the QD is saturated.

Figure 2(b) shows the RE intensities of the exciton and the positive trion as a function of the optical gate power in the restricted range 0.007–2 nW. In this range the nonresonant photoluminescence excited by the gate is completely negligible. For gate powers smaller than 0.5 nW, the trion RE increases with gate power indicating that the residual QD occupation evolves from two to one residual holes. For gate powers larger than 0.5 nW the trion RE saturates before a preliminary decrease, the QD becoming empty.

We have seen that the optical gate substantially modifies the QD population, we will now consider the consequences related to the QD electrostatic environment.

E. Energy of the resonant emission versus the optical gate power

Figure 3 displays the RE energies of the neutral exciton, E_X [Fig. 3(a)], and the positive trion, E_{X^+} [Fig. 3(b)], as a function of the optical gate power P_{gate}. The solid lines are obtained from the theoretical model described in details in the next section. A red shift of a few μeVs is first observed in the very weak gate power regime, followed by a comparable blue shift when the gate power increases. The transition between the red and blue shift occurs at a typical power of $P_{\text{gate}} \sim 0.05$ nW. This optical gate power is much smaller than the gate powers corresponding to the maximum RE intensities of the exciton ($P_{\text{gate}} \sim 3$ nW) and the trion ($P_{\text{gate}} \sim 0.5$ nW). In fact, the energy shifts of X and X^+ are governed, through the quantum confined Stark effect, by the charge state of the QD environment, while the RE intensity only depends on the charge state of the QD itself. This point will be quantitatively addressed in the next section.

IV. THEORETICAL MODEL OF THE OPTICAL GATE EFFECT

In the following, we propose a simple theoretical model which describes the processes involved in the quenching of the neutral exciton RE and the operation of the optical gate.

A. Population evolution without the optical gate

As explained in the Appendix, the residual doping of the sample is at the origin of a hole reservoir which will notably influence the QD emission. As we do not have a precise knowledge of the QD electrostatic environment, we simplify the general description of the influence of the residual doping on the QD charge state by considering an effective model where the distribution of holes at the vicinity of the QD is schematized by a single trap such as an interface defect of the wetting layer (see Fig. 4). Residual holes introduced by the nonintentional doping of the sample will preferably be trapped (de-trapped) in (from) the defect, and the corresponding capture (escape) rate is denoted R_C (R_E). For the sake of simplicity, each QD is supposed to be coupled to only one defect (the phenomenology is the same in case of more defects). This defect is located in the vicinity of the QDs and a tunneling channel between the defect state Φ and the QD fundamental hole state S_h opens if the defect is close enough to the QD (the distance between the QD and the interface defect is discussed in Sec. V B). The hole tunneling rate from the defect to the QD is denoted γ_{in}, and γ_{out} for the inverse process rate. Because the confinement of an interface defect is generally small, the Φ state is close to the valence band continuum and we assume that $\gamma_{\text{in}} \gg \gamma_{\text{out}}$. Finally, due to the spin of the carriers, the defect state Φ and the QD fundamental electron and heavy hole states, S_e and S_h, are twice degenerated and can then be populated by up to two carriers. From our experimental observations and from the calculation developed in the Appendix, this assumption seems reasonable since, without any light illumination, the S_h state of the QD is populated in average by two holes at most.

Within these hypotheses, the evolutions of the average number of holes in the defect, n_p, and the average number of holes (electrons) in the QD, n_h (n_e), are described by the rate equations:

$$\frac{dn_p}{dt} = R_C(2 - n_p) - R_E n_p - \gamma_{\text{in}}(2 - n_h)n_p$$
$$+ \gamma_{\text{out}}(2 - n_p)n_h, \tag{1a}$$
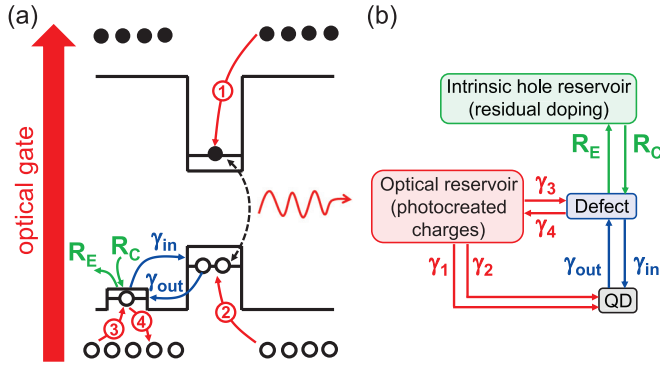
FIG. 5. (Color online) (a) Sketch of the optical gate effect: Carriers are created in the GaAs barrier and captured by the QD or the defect. (b) The capture and escape processes induced by the optical gate are schematized in a diagram showing the optical reservoir formed by the charges photocreated in the GaAs barrier by the optical gate.

$$\frac{dn_h}{dt} = \gamma_{\text{in}}(2 - n_h)n_p - \gamma_{\text{out}}(2 - n_p)n_h, \quad (1b)$$

$$\frac{dn_e}{dt} = 0. \quad (1c)$$

Considering $\gamma_{\text{in}} \gg \gamma_{\text{out}}$, the populations in the steady state are then given by $n_p^{(\text{st})} = 2R_C/(R_C + R_E)$, $n_h^{(\text{st})} \approx 2$, and $n_e^{(\text{st})} = n_e = 0$, where two holes populate the S_h state with the corresponding QD fundamental state $|2_h; 0_e\rangle$. Therefore, the absorption of a photon at the energy of the neutral exciton, for which the ground state $|g\rangle$ is $|0_h; 0_e\rangle$, is impossible and an inhibition of the neutral exciton RE is observed. *A priori,* such a configuration does not allow the absorption of a photon at the energy of the positive trion, which is associated with the fundamental state $|1_h; 0_e\rangle$, and the trion RE should not be observed contrarily to what is shown in Fig. 1(c). However, $n_p^{(\text{st})}$ and $n_h^{(\text{st})}$ are only the average numbers of carriers in the steady state, and, in the dynamical regime, fluctuations of n_p and n_h associated with a hole exchange between the QD and the defect exist. Therefore, even though the QD ground steady state is $|2_h; 0_e\rangle$, the $|1_h; 0_e\rangle$ state is sometimes reachable when a hole escapes from the QD to the defect. The resonant excitation of X^+ then becomes possible with nevertheless a low efficiency.

This elementary model explains the phenomenology of the quenching of the neutral exciton RE while the trion RE can be observed. In the next section, we improve this model in order to obtain a quantitative description of the optical gate effect.

B. Population evolution with the optical gate

The optical gate populates the GaAs barrier as described in Fig. 5 in the absence of the resonant excitation laser. The evolution of the average number of holes in the defect, n_p, in the QD, n_h, and the average number of electrons in the QD, n_e, is now described by the following rate equations:

$$\frac{dn_p}{dt} = R_C(2 - n_p) - R_E n_p - \gamma_{\text{in}}(2 - n_h)n_p$$
$$+ \gamma_{\text{out}}(2 - n_p)n_h + \gamma_3(2 - n_p) - \gamma_4 n_p, \quad (2a)$$

$$\frac{dn_h}{dt} = \gamma_{\text{in}}(2 - n_h)n_p - \gamma_{\text{out}}(2 - n_p)n_h$$
$$+ \gamma_2(2 - n_h) - \gamma n_h n_e, \quad (2b)$$

$$\frac{dn_e}{dt} = \gamma_1(2 - n_e) - \gamma n_h n_e, \quad (2c)$$

where γ_1 stands for the electron capture in the QD and γ_2 the hole capture rate in the QD, both from the barrier. The rates γ_3 and γ_4 correspond to the hole capture and escape for the defect, respectively. Since we study QDs in the strong confinement regime, the carriers trapped in the QD form electron-hole pairs in Coulomb interaction characterized by a relatively small binding energy compared to the kinetic energy resulting from the geometric confinement. In this context and in case of a low gate power for which the QD is hardly populated by more than one electron-hole pair in the fundamental state, the radiative recombination of an electron-hole pair in the QD at the neutral exciton energy is proportional to $n_e n_h$ when spin effects are not considered. The related radiative recombination rate γ corresponds to an excitonic radiative lifetime $T_1 = 330$ ps, which has been measured by time-resolved photoluminescence experiments in the same experimental configuration.[24]

In the explored power range, we assume the following hierarchy between the rates in the set of equations (2):

$$R_C, R_E, \gamma, \gamma_1, \gamma_2, \gamma_3, \gamma_4 \gg \gamma_{\text{in}} \gg \gamma_{\text{out}}. \quad (3)$$

This assumption will be justified in the following (see Sec. V C 1). Within this hypothesis, the variations of the QD charge state are essentially governed by the two capture processes (1) and (2), and its radiative recombination. Concerning the defect charge state, it is governed by the two capture processes from the barrier and from the hole reservoir (γ_3 and R_C), and the corresponding two escape processes (γ_4 and R_E).

Consequently, in the absence of the resonant excitation laser, the evolution of the charge states of the QD and the defect becomes independent when the optical gate is switched on, and the set of Eq. (2) is reduced to

$$\frac{dn_p}{dt} = R_C(2 - n_p) - R_E n_p + \gamma_3(2 - n_p) - \gamma_4 n_p, \quad (4a)$$

$$\frac{dn_h}{dt} = \gamma_2(2 - n_h) - \gamma n_h n_e, \quad (4b)$$

$$\frac{dn_e}{dt} = \gamma_1(2 - n_e) - \gamma n_h n_e. \quad (4c)$$

C. Excitonic complexes population evolution

In fact, under resonant excitation, Eqs. (4b) and (4c) are not satisfied since they do not take into account the electron and hole populations that are created by the resonant excitation laser. In this context, the QD charge state drastically modifies the absorption of the resonant excitation laser. We stress that the model is developed for resonant excitation powers where the resonance fluorescence contribution in the RE overwhelms the resonant Rayleigh scattering.[26] We thus focus on the populations and do not take into account any coherent effect. Moreover, the model describes the linear regime before
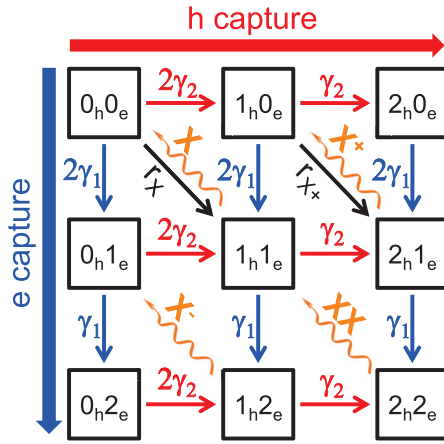
FIG. 6. (Color online) Diagram of the population evolution model.

the saturation of the QD by the resonant laser, which corresponds to the actual experimental configuration. Therefore, this model is only valid for intermediate powers of the resonant excitation laser, where stimulated emission processes are not considered, corresponding to its weak coupling regime with the QD (i.e., the strong coupling regime between the resonant laser and the QD, characterized by the so-called Mollow triplet, is not considered). Finally, this model is suitable for a nonresonant optical gate where the photocreated holes and electrons are not correlated.

In order to consider the different carrier populations in the QD, we adopt a population evolution model similar to the one proposed by Gomis-Bresco *et al.*,[35] which adapts for excitons the random population model of Grundmann *et al.*[36] Within this approach, all the processes related to the

charge capture, the radiative recombination, and the resonant pumping are taken into account by considering all the possible charge configurations of the QD. We restrict ourselves to the neutral exciton X, the positive and negative trions $X^{\pm}$, and the biexciton XX. These processes are schematized in Fig. 6, where the radiative recombination rates of these states are, respectively, denoted γ_X, $\gamma_{X^{\pm}}$ and γ_{XX} with $\gamma_X = \gamma_{X^{\pm}} \equiv \gamma$ and $\gamma_{XX} = 2\gamma_X$.[35] The resonant pumping rates at the energy of the neutral exciton X and the positive trion X^+ are denoted r_X and r_{X^+}, respectively, and depend on the power and the wavelength of the resonant excitation laser. Depending on the experimental configuration (i.e., resonant excitation of X or X^+), either r_X or r_{X^+} are set to zero in order to consider the resonant excitation of only one of these states. The probability $\mathcal{P}_{i_h;j_e}$ ($i,j = 0,1$, and 2) to obtain i_h holes and j_e electrons in the QD is calculated by replacing Eqs. (4b) and (4c) by the following linear differential equations system:

$$\frac{d\mathcal{P}}{dt} = \mathcal{T}.P, \tag{5}$$

where

$$\mathcal{P} = \begin{pmatrix} \mathcal{P}_{0_h;0_e} \\ \mathcal{P}_{0_h;1_e} \\ \mathcal{P}_{0_h;2_e} \\ \mathcal{P}_{1_h;1_e} \\ \mathcal{P}_{1_h;2_e} \\ \mathcal{P}_{2_h;1_e} \\ \mathcal{P}_{2_h;2_e} \\ \mathcal{P}_{2_h;0_e} \\ \mathcal{P}_{1_h;0_e} \end{pmatrix} \quad \text{with} \quad \sum_{(m,n)} \mathcal{P}_{i_h;j_e} = 1, \tag{6}$$

and

$$\mathcal{T} = \begin{pmatrix} -2(\gamma_1 + \gamma_2) - r_X & 0 & 0 & \gamma & 0 & 0 & 0 & 0 & 0 \\ 2\gamma_1 & -(\gamma_1 + 2\gamma_2) & 0 & 0 & \gamma & 0 & 0 & 0 & 0 \\ 0 & \gamma_1 & -2\gamma_2 & 0 & 0 & 0 & 0 & 0 & 0 \\ r_X & 2\gamma_2 & 0 & -(\gamma + \gamma_1 + \gamma_2) & 0 & 0 & \gamma & 0 & 2\gamma_1 \\ 0 & 0 & 2\gamma_2 & \gamma_1 & -(\gamma_2 + \gamma) & 0 & 0 & 0 & 0 \\ 0 & 0 & 0 & \gamma_2 & 0 & -(\gamma + \gamma_1) & 0 & 2\gamma_1 & r_{X^+} \\ 0 & 0 & 0 & 0 & \gamma_2 & \gamma_1 & -\gamma & 0 & 0 \\ 0 & 0 & 0 & 0 & 0 & 0 & 0 & -2\gamma_1 & \gamma_2 \\ 2\gamma_2 & 0 & 0 & 0 & 0 & \gamma & 0 & 0 & -(2\gamma_1 + \gamma_2) - r_{X^+}. \end{pmatrix} \tag{7}$$

The evolution of any charge state can be calculated in order to explain the RE signal observed at low or high power of the optical gate. Nevertheless, the validity of this model is limited to the case where the tunnel effect between the QD and the defect is negligible, meaning that the ultralow power regime, where γ_{in} and γ_{out} are comparable to γ_1 and γ_2, cannot be explained here.

V. THEORY VERSUS EXPERIMENTAL RESULTS

A. Photoluminescence and resonant emission dependence on the optical gate power

In our model, the intensity of the photoluminescence nonresonantly excited by the optical gate, I_X^{PL}, is proportional to the population of the QD state $|1_h; 1_e\rangle$ with resonant
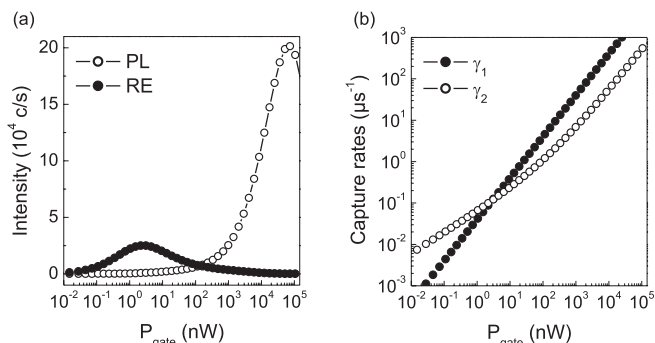
FIG. 7. (a) Results of the simulation showing the resonant emission (RE) and the nonresonant photoluminescence (PL) intensities of the neutral exciton as a function of the optical gate power P_{gate}. (b) Electron and hole capture rates, γ_1 and γ_2, as a function of the optical gate power P_{gate}.

pumping rates equal to zero, leading to

$$I_X^{\text{PL}} \propto \langle \mathcal{P}_{1_h;1_e} \rangle_{(st)} \big|_{r_X=r_{X^+}=0}. \tag{8}$$

The optically gated RE of the exciton, I_X^{RE}, is proportional to the difference of populations in the QD state $|1_h; 1_e\rangle$ with and without a resonant pumping $r_X = r$, such as

$$I_X^{\text{RE}} \propto \langle \mathcal{P}_{1_h;1_e} \rangle_{(st)} \big|_{r_X=r,\, r_{X^+}=0} - \langle \mathcal{P}_{1_h;1_e} \rangle_{(st)} \big|_{r_X=r_{X^+}=0}. \tag{9}$$

Likewise, the RE of the positive trion, $I_{X^+}^{\text{RE}}$, is defined from the population difference in the QD state $|2_h; 1_e\rangle$ with and without a resonant pumping $r_{X^+} = r$, such as

$$I_{X^+}^{\text{RE}} \propto \langle \mathcal{P}_{2_h;1_e} \rangle_{(st)} \big|_{r_X=0,\, r_{X^+}=r} - \langle \mathcal{P}_{2_h;1_e} \rangle_{(st)} \big|_{r_X=r_{X^+}=0}. \tag{10}$$

The two first Eqs. (8) and (9) are used to reproduce the experimental results in Figs. 2(a) and 2(b) and Eq. (10) is used to reproduce the RE arising from the trion in Fig. 2(b). The results of the simulation, presented in Figs. 2(b) and 7(a) are obtained with the four following parameters:

$$\begin{aligned}
r &= 15 \ \mu\text{s}^{-1} \\
\gamma &= 1/T_1 = 3030 \ \mu\text{s}^{-1} \\
\gamma_{1(\mu\text{s}^{-1})} &= 0.04\, P_{\text{gate(nW)}} \\
\gamma_{2(\mu\text{s}^{-1})} &= 0.06\sqrt{P_{\text{gate(nW)}}} + 0.005\, P_{\text{gate(nW)}}.
\end{aligned} \tag{11}$$

In fact, the experimental results depicted in Figs. 2(a) and 2(b) only allow one to determine the ratio γ_1/γ_2. The absolute values of these parameters are deduced from additional photoncorrelation measurements that are presented in Sec. V D. By using these parameters, the PL and RE intensity dependencies on the gate power are fairly reproduced both for the exciton X or the trion X^+. We stress here that the values of the above four parameters are used in all the simulations presented in the paper.

Let us now discuss the power dependence introduced for γ_1 and γ_2. Considering the evolution of the barrier electron (hole) population N_e (N_h) under a nonresonant excitation[37] and the fact that the photoluminescence of the GaAs barrier is not influenced by the QDs population,[38] the populations N_e and N_h created by the optical gate are governed by bimolecular interband radiative recombination[13,37] and are proportional to

$\sqrt{P_{\text{gate}}}$. The carriers can be then captured in the QD and the defect in its vicinity, either by the emission of optical phonons, or by Auger processes. The capture of a carrier in the QD by the emission of an optical phonon is a single charge process and is therefore proportional to the number of electrons or holes in the continuum,[1,2,39] and in other words to $\sqrt{P_{\text{gate}}}$. Contrarily to this latter process, the Auger-assisted capture of a carrier involves two charges, where the incident charge in the continuum interacts with a target charge either in the continuum [Auger effect of type (I)], or in the QD [Auger effect of type (II)]. Here, we consider Auger processes of type (I) because the type (II) processes are only efficient for a small range of QDs sizes.[3,4] The corresponding capture rate is then proportional to P_{gate}. Symmetrically to these capture processes, holes can escape from the defect by absorption of a phonon or by an Auger effect. De-trapping from the QD hardly occurs considering the high values of the hole and electron confinement energies (about 30 and 40 meV, respectively). Even though we do not have a precise knowledge of the electron and hole confinements in our sample, we assume that the carrier confinement is similar to the one in samples that were fabricated in the same facilities and which show a photoluminescence signal at the same excitonic energy (i.e., 1.27 eV).[40] In this type of sample, the confinement energy of the first electron (hole) state is larger (smaller) than the energy of an optical phonon so that the holes capture is, contrarily to the electrons, efficiently assisted by the emission of optical phonons. Moreover, regarding the linear power dependence of γ_1 and γ_2 at high gate powers when the nonresonant photoluminescence is observed, we conclude that the capture processes are completely governed by Auger processes. This observation is also in good agreement with the experimental work of Ohnesorge et al.[5] showing that the capture processes are mainly phonon assisted at low excitation density and Auger assisted at high excitation density.

In order to compare the capture rates used in our fits to the ones given in the literature,[2–4] the charge density has to be considered instead of the optical excitation power. Considering the number of electron-hole pairs created by the optical gate in the GaAs barrier $N = \sqrt{\frac{C}{\gamma_{\text{GaAs}}}}\sqrt{P_{\text{gate}}}$,[13,37] with C the photogeneration coefficient and γ_{GaAs} the radiative recombination rate of the electron-hole pairs in the GaAs barrier which are, respectively, about 10^{10} nW^{-1}s^{-1} (for a HeNe laser at 1.96 eV) and 1 ns^{-1},[41] the density of charges photocreated in the GaAs barrier is given by $n_{(\text{m}^{-2})} \approx 10^{12}\sqrt{P_{\text{gate(nW)}}}$ (for a laser spot diameter of 2 μm). Therefore, the power laws of γ_1 and γ_2 can be rewritten as

$$\begin{aligned}
\gamma_1 &= C_e^{\text{Auger}} n^2 \\
\gamma_2 &= C_h^{\text{Auger}} n^2 + A_h^{\text{LO}} n,
\end{aligned} \tag{12}$$

where $C_e^{\text{Auger}} = 4 \times 10^{-20}$ m^4/s and $C_h^{\text{Auger}} = 5 \times 10^{-21}$ m^4/s are, respectively, the coefficients for the electron and the hole capture by Auger effect, and $A_h^{\text{LO}} = 6 \times 10^{-8}$ m^2/s is the coefficient for the hole capture by emission of optical phonons. The estimates of the Auger coefficients are in agreement with the calculations of Uskov et al.[3] which predict an Auger coefficient of 2×10^{-20} m^4/s, as well as with the calculations of Magnusdottir et al.[4] which give coefficients of 10^{-22}–10^{-20} m^4/s for InAs/GaAs QDs with a radius of 5–15 nm.

Concerning the phonon-assisted capture, our estimated value of A_h^{LO} is equivalent to the coefficient $\widetilde{A}_h^{LO} = e_{GaAs} A_h^{LO} = 1.8 \times 10^{-5}$ cm^3/s where the substrate thickness of the sample, $e_{GaAs} \approx 300$ μm, is taken into account. This value is also in perfect agreement with the calculations of Magnusdottir *et al.*[2] where $\widetilde{A}_h^{LO} = 3.8 \times 10^{-5}$ cm^3/s.

Figure 7(b) displays the dependence on the optical gate power P_{gate} of the capture rates γ_1 and γ_2, given by Eq. (11). When $P_{gate} < 3$ nW, i.e., $\gamma_1/\gamma_2 < 1$, an excess of holes and no electron populate the QD, and once P_{gate} increases, the ratio γ_1/γ_2 increases and the exciton RE signal increases. When $P_{gate} = 3$ nW, i.e., $\gamma_1/\gamma_2 = 1$, the QD is completely neutralized due to the symmetrical electron and hole capture rates, and the RE signal is maximum. It should be noted that the dynamical aspect of the process should not to be forgotten. When $P_{gate} > 3$ nW, i.e., $\gamma_1/\gamma_2 > 1$, an excess of electrons and no hole populate the QD, and once P_{gate} increases, the ratio γ_1/γ_2 increases and the exciton RE signal vanishes. The RE of the negative trion should then be observed. However, the bandwidth of the microcavity is not wide enough to detect any signal from this latter excitonic complex which is characterized by a typical binding energy of the order of 7 meV for InAs/GaAs QDs emitting at 1.27 eV.[42]

To conclude this section, the experimental study of the exciton RE over seven orders of magnitude of the gate power led to the determination of the nature of the carrier capture processes involved in a QD. While other groups[1,35] have previously used the nonresonant photoluminescence to evaluate the carriers capture rates, we benefit here from the resonant excitation and its optical gating effect to probe the QD ground state, which is determined by the capture of the electrons and holes created by the nonresonant laser. In particular, this method gives access to ultraslow capture processes in the very low gate power regime where the nonresonant photoluminescence is completely negligible. Inversely, when the nonresonant photoluminescence is observed, the capture rates are already at least of the order of 1 ns^{-1}.[35] In the context of our unusual experiments, the population model that we used allows us to estimate the capture rates γ_1 and γ_2 which vary from a few ms^{-1} to a few hundred ps^{-1} in the explored power range (i.e., seven orders of magnitude). Finally, it should be noted that the estimations of γ_1 and γ_2 are in very good agreement with the theoretical calculations of the capture processes assisted by the Auger effect and optical phonon emissions. This study allows a first comprehensive confrontation between theory and experiment concerning the carrier capture in QDs.

B. Energy shifts of the neutral exciton and the positive trion

The electric field created by a hole trapped in the vicinity of the QD induces, through the quantum confined Stark effect, energy shifts Δ_X on E_X and Δ_{X^+} on E_{X^+}. The Stark effect is here induced by Coulomb interactions between the hole in the defect and the carriers in the QD, and Δ_X and Δ_{X^+} are obviously very sensitive to the relative position of the defect to the QD.[43,44] The energy shift of the X and X^+ RE further depends on the number of holes in the defect and are simply given by

$$\delta E_X = n_p^{(st)} \Delta_X \quad \text{and} \quad \delta E_{X^+} = n_p^{(st)} \Delta_{X^+}, \tag{13}$$

where $n_p^{(st)} = 2 - \frac{2}{1 + \frac{R_C + \gamma_3}{R_E + \gamma_4}}$ is the number of holes in the defect in the steady-state regime, given by the rate Eq. (4a).

The experimental results in Fig. 3 are fitted with the expressions of E_X and E_{X^+} of Eq. (13) by adjusting the following parameters:

$$\Delta_X = 7 \ \mu\text{eV} \quad \text{and} \quad \Delta_{X^+} = 5 \ \mu\text{eV}$$
$$R_C = 1/30 \ \mu\text{s}^{-1} \quad \text{and} \quad R_E = 1/60 \ \mu\text{s}^{-1}$$
$$\gamma_{3(\mu\text{s}^{-1})} = 1/3 P_{gate(nW)}$$
$$\gamma_{4(\mu\text{s}^{-1})} = 0.3 \sqrt{P_{gate(nW)}}. \tag{14}$$

Thoroughly, the values of R_C and R_E are deduced from the study of the charge dynamics in the transient regime when the optical gate is switched off, presented in Sec. V C1. Consequently, knowing these values allows us to determine the power dependence of γ_3 and γ_4. We deduce that the defect is never empty, even in the absence of the optical gate for which its steady state is characterized by $n_p^{(st)}|_{min} = n_p^{(st)}|_{\gamma_3 = \gamma_4 = 0} \approx 1$. The modification of the number of holes mainly happens in the very low optical gate power regime (i.e., $P_{gate} < 10$ nW). Here, the red shift corresponds to a decrease of the number of holes in the defect whereas the blue shift is related to an increase of holes. The estimated values of Δ_X and Δ_{X^+} are used to evaluate the distance between the defect and the QD. Referring to the theoretical calculations of Jankovic *et al.* of the Stark effect induced by a hole in the wetting layer,[43] these shifts correspond to a distance of 20–25 nm between the interface defect and the QD, which is also in good agreement with the work of Abbarchi *et al.*[44] This distance is large enough to avoid any overlap between the wave functions of the holes in the defect and in the QD. In other words, the holes are localized in the defect, resulting in small capture and escape rates R_C and R_E.

We also explain that once the optical gate is turned on, the charge states of the defect and of the QD are no longer coupled since the tunneling channel becomes negligible (see Sec. IV B). Therefore, the variations of the energies E_X and E_{X^+} are not correlated with the intensity variations of the X and X^+ RE signals.

Finally, we discuss the power dependencies of the rates γ_3 and γ_4. For the trapping rate of holes in the defect γ_3, since the confinement energy of an interface defect E_Φ is very low, the hole capture by Auger effect is very efficient. The trapping rate γ_3 depends then essentially on Auger processes which are 60 times more efficient than the holes capture in the QD. Concerning the de-trapping rate γ_4 of holes from the defect to the continuum reservoir, either phonons absorption, or Auger processes involving one incident charge in the barrier and one target charge in the defect[1,45,46] which explain the square root power dependence, can be considered. On the one hand, the phonon-assisted mechanism would concern the absorption of acoustic phonons because the optical phonon states are not populated at low temperature.[46] Moreover, contrarily to the case of charges trapped in the QD, the de-trapping from the defect by absorption of an acoustic phonon can be efficient due to the smaller confinement of the order of 10 meV which is comparable to the typical energy of the acoustic phonons involved with confined states. On the other hand, various experimental studies showed that the fluctuating electrostatic

environment, related to the trapping and de-trapping of charges in defects close to a QD, is notably responsible for the zero-phonon line broadening in QDs at low temperature.[13,46] In such a context, the de-trapping of charges from the defects is driven by Auger effects, which are also very efficient for trapping holes in defects. We thus assume that γ_4 is, as γ_3, preferentially associated with Auger-assisted de-trapping processes, where one hole in the defect interacts with another hole in the barrier, than to the absorption of acoustic phonons.

C. Study of the charges dynamics in the transient regime

In the previous sections, we have studied the influence of the optical gate power on the intensity and the energy of the RE signal, which led one to analyze, in the steady-state regime, the charge state of the QD and of the interface defect in its vicinity, respectively. In the corresponding experiments, the optical gate is always switched on and the physical properties are average values in the steady-state regime. In this section, we focus on the dynamics of the optical gate effect by studying the transient regimes where the optical gate has just been switched on or off. We consider two situations: the OFF stage when the optical gate is turned off at $t = 0$, knowing that the system was in a steady state with the applied gate at $t < 0$, and the ON stage when the optical gate is switched on at $t = 0$, knowing that the system without the applied gate was in a steady state at $t < 0$.

Experimentally, we send two light beams. The first one, provided by the tunable cw external cavity laser diode, resonantly excites the excitonic transition, while the second one is our optical gate (HeNe laser), which is modulated from 0 to a few nWs at 400 Hz by using an acousto-optic modulator. An oscilloscope records a time histogram of the RE where each detected photon corresponds to one event. The temporal resolution of the experimental setup is evaluated by measuring the system response for the two stages when the modulated optical gate is directly sent to the photodetector, and turns out to be 1.7 μs in the OFF stage and 2 μs in the ON stage.

1. OFF stage

Under resonant excitation, two effects are responsible for the RE intensity variation when the optical gate is switched off at time $t = 0$: the energy shift of the transition which depends on the gate power as described in Secs. III E and V B, and the quenching of the exciton RE due to the charging of the QD by holes tunneled from the defect to the QD at a rate γ_{in}. These two phenomenons are governed by the time constants t_{shift} and t_{off} which affect the central energy of the transition and the recorded RE intensity, respectively. The physical meaning of these two times appears clearly when considering the RE spectrum, which can be recorded. For $t > 0$ and at a given detuning δ between the resonant excitation laser and the exciton energies, it can be modeled by a Lorentzian line:

$$I(\delta, t > 0) = \frac{I_0 e^{-t/t_{off}}}{[\delta - \Delta(1 - e^{-t/t_{shift}})]^2 + \Gamma'^2/4}. \quad (15)$$

One example of the temporal evolution of the neutral exciton RE is shown in Fig. 8(a), for an optical gate power of 3 nW, at $\delta = -1$ μeV. Two distinct features are observed
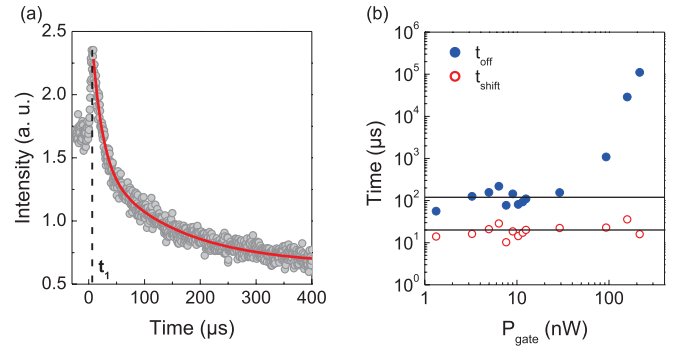
FIG. 8. (Color online) (a) Temporal evolution of the neutral exciton resonant emission when the optical gate is switched off at $t = 0$ ($P_{gate} = 3$ nW). The detuning between the resonant excitation laser and the exciton energies is equal to $\delta = -1$ μeV. (b) Time constants t_{shift} and t_{off} as a function of the optical gate power P_{gate}.

in the experimental results. For $0 < t \leqslant t_1$, the exciton energy E_X decreases and it thus gets closer to the resonant laser energy E_L because of the initially chosen negative detuning. Therefore, the RE signal starts to increase. At $t = t_1$, the laser is strictly resonant with the excitonic transition and the RE signal is maximum. When $t > t_1$, the red shift phenomenon is still effective and the exciton energy E_X moves away from the resonant excitation laser energy E_L. The RE signal then first decreases with the time constant t_{shift}. Once the exciton energy reaches its limit ($t \gg t_{shift}$), the RE signal still slowly decreases with the time constant $t_{off} \gg t_{shift}$, really characteristic of the dynamics of the RE intensity. For $\delta = -1$ μeV, the experimental data are fitted [Fig. 8(a), solid line] by a double exponential decay with the time constants $t_{shift} = 20 \pm 1$ μs and $t_{off} = 150 \pm 10$ μs. Performing the same experiment for various detunings and optical gate powers allows a complete study of the variations of t_{off} and t_{shift} with the gate power, as well as a direct comparison with our theoretical model. The results that are presented in Fig. 8(b) first show that t_{shift} is relatively constant over the whole explored range of gate power ($P_{gate} \leqslant 200$ nW). For t_{off}, we observe also a relative constant value for $P_{gate} \leqslant 30$ nW followed by a strong increase once $P_{gate} \geqslant 100$ nW, until a remarkable value of 20 ms for $P_{gate} \sim 200$ nW.

When the optical gate is switched off, the remaining photogenerated carriers in the barrier can relax through two channels: a direct radiative recombination of the electron-hole pairs with a radiative lifetime of about 1 ns,[41] and a nonradiative relaxation towards the QDs or the defects with time constants of the order of 10 μs (given by the capture rates values γ_1, γ_2, γ_3 at $P_{gate} = 3$ nW, and R_C). Since for ultralow carrier populations, such as the ones we consider now, the second channel is much less efficient than the first one, we assume that, for an initial very low gate power, after switching off the optical gate, the barrier empties almost instantaneously by radiative recombination of the electron-hole pairs. In other words, neither a modification of the charge state of the QD nor of the defect is induced by the GaAs barrier. The charge state of the QD and of the defect can then be described as follows.

The hole population in the defect at anytime t is deduced from the rate Eq. (1a), where γ_{in} and γ_{out} are neglected with

respect to the trapping and de-trapping rates R_C and R_E, and is given by

$$n_p(t) \approx \left(n_p(0) - \frac{2R_C}{R_C + R_E}\right)e^{-(R_C+R_E)t} + \frac{2R_C}{R_C + R_E}.$$

$$(16)$$

When the optical gate is switched off, the defect relaxes to its steady state defined by $n_p^{(st)} = 2R_C/(R_C + R_E)$. Since the neutral exciton energy is defined as $\delta E_X(t) = n_p(t)\Delta_X$ [see Eq. (13)], E_X is time dependent and follows an exponential law with a time constant $t_{shift} = (R_C + R_E)^{-1}$. This energy shift can be either a red shift or a blue shift depending on the initial gate power.

As far as the QD population is concerned, when the optical gate is turned off, the hole transfer to the QD is ensured by the tunneling channel between the QD and the defect which is not negligible anymore since there are no more charges in the barrier. Moreover, since $\gamma_{out} \ll \gamma_{in} \ll R_C, R_E$, the hole capture in the QD is much slower than the recovery of the defect's equilibrium. Therefore, we can assume that the number of holes in the defect has already reached its steady-state value $n_p^{(st)}$ when the number of holes in the QD starts to increase. The rate Eq. (1b) then leads to the following hole population in the QD at anytime t:

$$n_h(t) \approx 2 - (2 - n_h(0))e^{-\gamma_{in}n_p^{(st)}t},$$

$$(17)$$

where the hole transfer to the QD is done at a rate $\gamma_{in}n_p^{(st)}$ which defines the time constant $t_{off} = (\gamma_{in}n_p^{(st)})^{-1}$. When the optical gate is turned off, the QD hole population relaxes to its steady-state value defined by $n_h^{(st)} \approx 2$.

To summarize, in the context of an initial ultraweak optical gate, the time constants t_{shift} and t_{off} are given by

$$t_{shift} = \frac{1}{R_C + R_E} \quad \text{and} \quad t_{off} = \frac{1}{\gamma_{in}}\frac{R_C + R_E}{2R_C}. \quad (18)$$

Let us first consider the large increase of t_{off} for initial gate powers larger than 100 nW. The initial carrier population in the barrier starts to be sufficiently large so that our main hypothesis of an instantaneously emptied barrier through radiative recombination breaks down. An increasing amount of carriers relax towards the QD and the defect, substantially altering the charging dynamics of the QD. We emphasize that the direct relaxation of electrons towards the QD will essentially slow down the retrieval of the equilibrium situation. For gate powers smaller than 100 nW, the measurement of the time constant $t_{shift} \approx 20$ μs [average value as a solid line in Fig. 8(b)] allows to estimate the values of $R_C = 1/30$ μs^{-1} and $R_E = 1/60$ μs^{-1} which were presented previously in Sec. V B.

Let us now come back to the hierarchy introduced for the relaxation rates in Sec. IV B [Eq. (3)]. In the low optical gate power regime, the knowledge of the time constant $t_{off} \approx 120$ μs [average value as a solid line in Fig. 8(b)] allows one to give an estimate of the capture rate from the defect to the QD, which turns to be $\gamma_{in} \approx 1/160$ μs^{-1} (and $\gamma_{in} \gg \gamma_{out}$ at low temperature). Considering the estimate of $R_C = 1/30$ μs^{-1}, $R_E = 1/60$ μs^{-1}, and $\gamma_1 \approx 1/25$ μs^{-1}, $\gamma_2 \approx 1/15$ μs^{-1}, $\gamma_3 \approx 1/3$ μs^{-1}, and $\gamma_4 \approx 1/3$ μs^{-1} for a typical small gate power $P_{gate} \approx 1$ nW, Eq. (3) is verified.
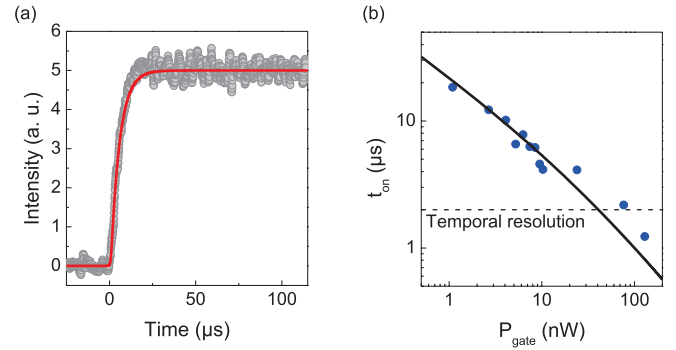
FIG. 9. (Color online) (a) Temporal evolution of the neutral exciton resonant emission when the optical gate is switched on at $t = 0$ ($P_{gate} = 10$ nW). The detuning between the resonant excitation laser and the exciton energies is equal to $\delta = -1$ μeV. (b) Time constant t_{on} as a function of the optical gate power P_{gate}. The theoretical fit (solid line) is given by the power laws (11) of the capture rates γ_1 and γ_2.

Moreover, since all these rates (except R_C and R_E which are constant) increase with gate power, the hierarchy introduced previously is fulfilled for a large range of gate powers, at least corresponding to our experimental conditions.

2. ON stage

We now present the same set of measurements for the ON stage. Figure 9(a) shows an example of the temporal evolution of the neutral exciton RE when the optical gate is switched on ($P_{gate} = 10$ nW), at the same detuning $\delta = -1$ μeV chosen for the OFF stage experiment. For $t < 0$, the detected signal is negligible since the optical gate is switched off, whereas for $t > 0$, the RE signal increases very quickly as soon as the optical gate is switched on. Contrarily to the OFF stage, no energy shift of the exciton is observed. Indeed, as described in Sec. IV (see Fig. 5), when the optical gate is switched on, the charge state in the defect is mainly governed by the trapping and de-trapping processes (3) and (4) characterized by the time constants $\gamma_3^{-1} \sim 0.1$ μs and $\gamma_4^{-1} \sim 1$ μs at $P_{gate} = 10$ nW [Eq. (14)]. With such time scales, as the time resolution of our gate modulation experiment is limited to 2 μs, the intensity rise induced by the energy shift is beyond our detection limit. The experimental data in Fig. 9(a) are well fitted by the convolution of one exponential with a time constant $t_{on} = 5 \pm 1$ μs and the system time response of 2 μs.

We now consider the dependence of t_{on} on the optical gate power, shown in Fig. 9(b). The time constant t_{on} decreases with increasing P_{gate}. Indeed, the appearance of the RE signal once the optical gate is turned on is related to the capture processes (1) and (2) characterized by the rates γ_1 and γ_2 which vary with the optical gate power (see Sec. V A). We then expect that the time constant t_{on} strongly depends on P_{gate}. Thanks to the resolution of the linear differential system (5) developed within the population evolution model and the expressions (11) of γ_1 and γ_2, we deduce that $t_{on} = \frac{3}{2(\gamma_1 + \gamma_2)}$. We see in Fig. 9(b) that this latter expression fits well our experimental data.
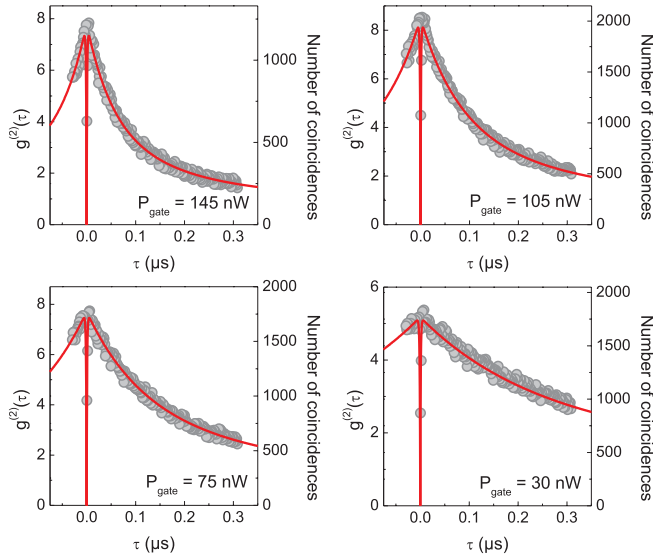
FIG. 10. (Color online) Intensity autocorrelation measurements of the optically gated resonant emission of the neutral exciton, for four optical gate powers (taken from a complete study over 12 gate powers). The experimental data correspond to the number of coincidences as a function of the time delay while the theoretical curves, results of the population evolution model, are plotted on a dual scale by adjusting the experimental and theoretical maxima. The parameters used in the theoretical model are $\gamma = 3030 \ \mu s^{-1}$, $r_X = 500 \ \mu s^{-1}$. γ_1 and γ_2 are given by the power laws (11).

D. Photon autocorrelation

1. Experimental results

In order to study the photon statistics of the optically gated RE of the neutral exciton, the intensity autocorrelation function of the emitted photons is measured by using a conventional Hanbury-Brown and Twiss setup. This experiment is done when the QD is in its steady state (i.e., the optical gate is always turned on) for various optical gate powers in the range 20–200 nW. The results of four measurements (over a set of 12 measurements) are presented in Fig. 10. Even if the time window has a width of 350 ns, which is large for photon correlation experiments in InAs/GaAs QDs,[14,47,48] it appears not large enough to observe the limit value of the number of coincidences at long time scales, and therefore, the data normalization becomes tricky. To overcome this problem, the raw experimental data are plotted in the unit of the number of coincidences as a function of the time delay τ. Another consequence of this large time window is the poor resolution of the experimental antibunching dip observed at zero delay.

The antibunching at zero delay is the signature that the RE signal corresponds to the single photon emission from the QD.[26] Apart from zero delay, on all spectra, a strong bunching appears, up to values of $g^{(2)}(\tau) = 8$ for $P_{gate} = 145$ nW. We note that this bunching decays with a time constant $\tau_B \sim 0.1 \ \mu s$ (for $P_{gate} = 145$ nW), much longer than the radiative lifetime $T_1 = 330$ ps of the QD. In fact, the $g^{(2)}(\tau)$ function reflects the population dynamics of the neutral exciton state which is given, in our model, by the probability $\mathcal{P}_{1_h;1_e}$. This dynamics is driven not only by the radiative recombination but also by the capture processes occurring on very long times
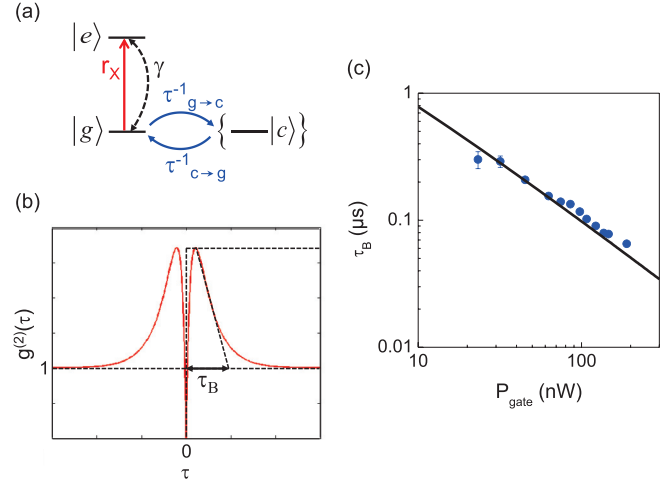
FIG. 11. (Color online) (a) Sketch showing the fluctuation of the quantum dot charge state and its resonant emission when the resonant laser and the optical gate are simultaneously switched on. (b) Trend of the second-order correlation function of the exciton resonant emission characterized by the bunching time constant τ_B. (c) Experimental values of the time constant τ_B characterizing the bunching decay as a function of the optical gate power P_{gate} (symbols) and theoretical curve corresponding to Eq. (21) (solid line).

γ_1^{-1} and γ_2^{-1}. As shown in the following, the capture rates of the carriers photogenerated in the barrier by the optical gate are responsible for the bunching phenomenon. Therefore, the order of magnitude of the measured time constant τ_B is given by γ_1^{-1} and γ_2^{-1}, and will give values of τ_B up to a few hundred nanoseconds.

2. Photon statistics of the resonant emission

In the regime of very low optical gate power, where $\gamma_1, \gamma_2 \ll \gamma$, the emitted photons come mostly from the RE because the nonresonant photoluminescence excited by the optical gate is negligible. However, the resonant laser only excites the QD if this latter is in its empty ground state $|0_h; 0_e\rangle$. Therefore, the photon statistics strongly depends on the QD charge state. As discussed in the theoretical model, the QD charge state fluctuates over time due to the charge capture processes (1) and (2) characterized by the rates γ_1 and γ_2. This fluctuation is completely described by our model with its nine possible charge states (see Fig. 6). As depicted in Fig. 11(a), once the QD is empty, the QD remains uncharged for a time $\tau_{g \rightarrow c}$. After a time $\tau_{g \rightarrow c}$, the QD evolves towards one of its charged states $\{|c\rangle\}$. The charged state $|c\rangle$ presents either an excess of electrons with no hole if $\gamma_1 > \gamma_2$ or an excess of holes with no electron if $\gamma_1 < \gamma_2$. From the scheme of Fig. 6, we obtain, in first approximation,

$$\tau_{g \rightarrow c}^{-1} \approx \begin{cases} 2\gamma_1 & \text{if} \quad \gamma_2 < \gamma_1 \ll \gamma \\ 2\gamma_2 & \text{if} \quad \gamma_1 < \gamma_2 \ll \gamma. \end{cases} \quad (19)$$

Similarly, the QD remains in a charged state $\{|c\rangle\}$ during a time $\tau_{c \rightarrow g}$ (the QD can evolve from one charged state to another). Since, in the regime of very low gate power, the disappearance of a hole (an electron) arises from the slow capture of an electron (a hole) followed by their fast radiative recombination, we deduce from Fig. 6 that the time constant

$\tau_{c \to g}$ is approximately given by

$$\tau_{c \to g}^{-1} \approx \begin{cases} 2\gamma_2 & \text{if } \gamma_2 < \gamma_1 \ll \gamma \\ 2\gamma_1 & \text{if } \gamma_1 < \gamma_2 \ll \gamma. \end{cases} \qquad (20)$$

Let us now discuss the way the QD charge state is probed by the resonant laser at a pumping rate r_X. Under resonant excitation, as soon as the QD is in its ground state $|g\rangle$, it is resonantly pumped to its excited state $|e\rangle$ [see Fig. 11(a)]. Once in the excited state, the QD emits a photon and ends up in its ground state. This cycle is repeated during the time $\tau_{g \to c}$ after which the QD evolves to a charged state $\{|c\rangle\}$, and the resonant laser can no longer excite the QD at the neutral exciton energy. The single photon emission is then blocked for the time $\tau_{c \to g}$ while the QD remains in a charged state. After $\tau_{c \to g}$, the QD is back to its ground state and the resonant laser plays its role again. Therefore, the QD emits packets of single photons with a statistics governed by the exchange dynamics between the ground state $|g\rangle$ and the charged states $\{|c\rangle\}$. We note that the time intervals characterizing the emission of the photon packets are very long compared to the QD radiative lifetime since $\gamma \gg \gamma_1, \gamma_2$.

The probability of detecting two photons for a delay τ of the order of the bunching time τ_B is high. It is possible to show that $\frac{1}{\tau_B} = \frac{1}{\tau_{g \to c}} + \frac{1}{\tau_{c \to g}}$[49,50] and thus, in our case,

$$\tau_B = \frac{1}{2(\gamma_1 + \gamma_2)}. \qquad (21)$$

The bunching time τ_B is obtained from an exponential fit of the experimental results for $g^{(2)}(\tau)$, as schematized in Fig. 11(b). Figure 11(c) shows the values obtained for τ_B as a function of the optical gate power. These values are in fair agreement with Eq. (21), where γ_1 and γ_2 are given by the power laws (11) presented in Sec. V A. This confirms the validity of our approach.

Moreover, the entire set of measurements of the intensity autocorrelation function can be fitted in the framework of our model. For the considered two-level system, where the excited state is the excitonic state $|1_h; 1_e\rangle$ and the ground state is the vacuum state $|0_h; 0_e\rangle$, the probability of detecting a single photon at delay τ is proportional to the population of the excited state at delay τ or in other words to the probability $\mathcal{P}_{1_h;1_e}(\tau)$. Likewise, the probability of detecting a single photon at zero delay is proportional to the probability of having the system in its ground state and consequently to the probability $\mathcal{P}_{0_h;0_e}(\tau = 0) = 1$, the others being set to zero. The $g^{(2)}(\tau)$ function can then be defined as the probability of detecting a photon at delay τ, knowing that a photon has been detected at zero delay, normalized to the total probability $\mathcal{P}_{1_h;1_e}^{(st)}$ of detecting a photon due to the X recombination:

$$g^{(2)}(\tau) = \left. \frac{\mathcal{P}_{1_h;1_e}(\tau)}{\mathcal{P}_{1_h;1_e}^{(st)}} \right|_{\mathcal{P}_{0_h;0_e}(\tau=0)=1}. \qquad (22)$$

The theoretical curves of $g^{(2)}(\tau)$, calculated with the previously determined γ_1 and γ_2 values, are displayed in Fig. 10. As already stated, our time window is not large enough to observe the limit value of the number of coincidences at long time scales and in Fig. 10 the number of recorded coincidences is plotted as a function of the delay. The maxima of the

experimental and theoretical curves are then displayed on a double scale. Once again we observe a good agreement between the experimental findings and the predictions of our model.

The measurements of the second order autocorrelation function allow one to establish a clear link between the observed bunching effect and the capture processes in the QD of the carriers that are photogenerated by the optical gate. Under resonant excitation, in the very low gate power regime, the single photon emission occurs during a characteristic time given by $\tau_{g \to c} \approx \frac{1}{\max(2\gamma_1, 2\gamma_2)}$ [Eq. (19)] and the time interval between two consecutive single photon packets is given by $\tau_{c \to g} \approx \frac{1}{\min(2\gamma_1, 2\gamma_2)}$ [Eq. (20)]. This induces a blinking effect of the RE. Such a behavior may be reminiscent of the one observed on the nonresonant photoluminescence in QDs and nanocrystals. Although slow bunching effects were observed, they arose from the so-called spectral diffusion effect.[13,49,51–53] In our case, the QD charge state fluctuations are the main reason for photon bunching[54,55] and we observe a blinking between distinct excitonic states, namely the neutral exciton and the other excitonic complexes. Note that a similar blinking behavior had already been observed in the differential transmission of a single QD under resonant excitation.[56]

VI. CONCLUSION

To summarize, we have shown that the electrostatic environment plays a crucial role on the optical response of a single QD even under resonant excitation where no charge is photocreated in its vicinity. A self-consistent calculation presented in the Appendix highlighted the influence of the unintentional residual carbon doping under no optical excitation which leads to the presence of at least one residual charge in the QD. As a result, more than 90% of the QDs present a complete quenching of the neutral exciton RE because of the Coulomb blockade effect. In this context, an additional weak nonresonant laser is used as an optical gate to control the QD charge state thanks to the capture of the photocreated charges in the GaAs barrier, resulting in the QD neutralization. The optical gate not only induces a complete retrieval of the neutral exciton RE, but also allows an efficient control of the RE in the original regime where the photoluminescence nonresonantly excited by the optical gate is completely negligible. We developed a population evolution model where the different capture and escape processes induced by the optical gate are considered to describe the dynamics of the QD charge state. This model perfectly fits, with only a single set of reasonable parameters, the various experimental results presented over seven orders of magnitude of the optical gate power, in the steady-state and dynamical regimes. It appears that the QD ground state, and thus the RE intensity, is governed by peculiar Auger- and optical phonon-assisted capture processes characterized by long relaxation times of the order of 1–100 μs. Moreover, the measurements of the capture coefficients for both processes are in good agreement with theoretical calculations of various research groups. This study then constitutes a first confrontation between theory and experiment with such a low dynamic, concerning the carrier capture in QDs. Finally, the slow capture processes can be directly associated with an intermittent behavior of the QD RE,

which is similar to the blinking effect in QDs and nanocrystals, and where the RE quenching will be observed as long as the QD ground state is a charged state. In summary, we presented an experimental and theoretical study where the optical gate acts as a very sensitive probe of the residual doping and the QD population in an unprecedented explored regime of weak nonresonant excitation.

ACKNOWLEDGMENTS

APPENDIX: INFLUENCE OF THE RESIDUAL DOPING ON THE CHARGE STATE OF THE QUANTUM DOT

According to the experiments, the sample has an unintentional residual carbon doping (C doping)[32] of volume density n_A. The carbon binding energy E_A is about 26.7 meV, so that thermal activation can be neglected at the temperature of the experiments (7 K). As a consequence, in absence of the QDs, the acceptors are neutral and the Fermi energy is pinned at the energy E_A above the top of the GaAs valence band. A QD introduces bound states well above this energy, and thus some holes transfer towards the QDs, leading to the formation of a depletion region around the QD plane [see Fig. 12(a)]. To estimate the density of transferred holes, we assume an idealized ensemble of identical QDs (of areal density n_{QD} around 10^8 cm^{-2}) uniformly distributed in the QD plane (taken at $z = 0$). Neglecting both the QD height along the growth axis [(0z) direction] and the structuration due to the Bragg mirrors, one obtains a volume charge distribution in the sample:

$$\rho(z) = \begin{cases} -en_A + ep_B\delta(z) & \text{for } |z| < l_A/2 < l_M/2 \\ 0 & \text{otherwise,} \end{cases} \quad \text{(A1)}$$

where l_A is the thickness of the depletion layer around the QD plane [Fig. 12(b)] and p_B the areal density of bound (to the QDs) holes. We assume that acceptors are present only in a finite region around the QD plane, of total thickness l_M (for definiteness, we consider the thickness of the epitaxially grown cavity and take $l_M \approx 10\,\mu$m in the calculations). Charge neutrality gives $n_A l_A = p_B$ if only part of the acceptors are ionized ($l_A < l_M$), or $n_A l_M = p_B$ if all holes from doping are transferred into the QDs ($l_A = l_M$). Finally, the one-dimensional Poisson equation imposes a red shift of the QD levels by

$$E_{SC} = -\frac{e^2 p_B^2}{8\epsilon_0 \epsilon_r n_A}, \quad \text{(A2)}$$

where $\epsilon_r = 12.5$ is the GaAs relative dielectric constant.

We consider that the QDs have cylindrical symmetry and, for the parameters in our sample, can bind up to six holes, distributed in the S and P shells (respectively, twice and fourfold degenerated, considering both orbital and spin degrees of freedom). The S and P single electron and hole states are initially variationally calculated for a QD of in-plane radius $R = 75$ Å and height $h = 15$ Å (for which one
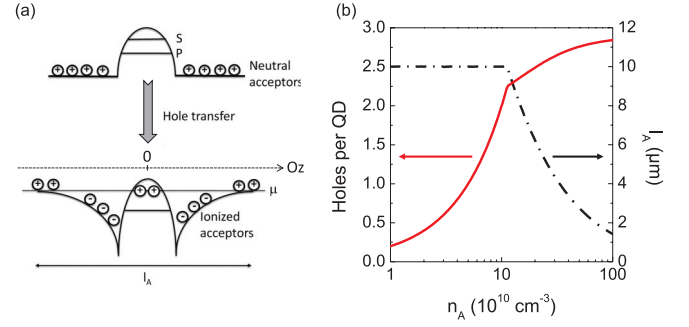
FIG. 12. (Color online) (a) (Top) Sketch along the growth direction (0z) of the valence band of an empty QD surrounded by neutral acceptors from the unintentional residual carbon doping. (Bottom) Sketch of the same QD after the acceptor ionization and the resulting hole transfer towards the QD. l_A is the thickness of the depletion region around the QD plane and μ the chemical potential fixed to the Fermi energy of the neutral acceptors outside the depletion region. (b) Hole occupancy and depletion length l_A as a function of the bulk doping density n_A, for a QD density $n_{QD} = 5 \times 10^7$ cm^{-2}, at $T = 7$ K.

calculates $E_X \approx 1274$ meV). The one-hole states are then used for the calculation of the Coulombic-correlated (and fully antisymmetrized) hole states of the multicharged QD (hosting $N = 2, \ldots, 6$ holes; for details see Ref. 57). Finally, we evaluate the average hole occupancy per QD:

$$\frac{p_B}{n_{QD}} = \frac{\sum_N N \sum_{n(N)} \exp[\beta(N\mu - E_{n(N)})]}{\sum_N \sum_{n(N)} \exp[\beta(N\mu - E_{n(N)})]}, \quad \text{(A3)}$$

where $E_{n(N)}$ is the energy of the nth state of the QD with N holes ($N = 0, 1, \ldots, 6$), $1/\beta = k_B T$, and μ is the chemical potential. Self-consistency of the hole occupancy is obtained by rigidly red-shifting the one-hole energies entering in the calculations of $E_{n(N)}$ by E_{SC} [Eq. (A2)]. Finally, the value of μ is either imposed to be equal to the energy of holes bound to the acceptors outside the depletion region if the transfer is partial ($l_A < l_M$), or should be found is a self-consistent way when the transfer is maximum ($l_A = l_M$).

Figure 12(b) shows the calculated hole occupancy (left scale) and depletion layer thickness (right scale) as a function of the bulk doping density n_A (at $T = 7$ K) and for a QD density of 5×10^7 cm^{-2}. We clearly observe the consecutive filling of the various valence-band shells with increasing acceptor density. It is worth stressing that at low doping densities, all holes transfer to the QD plane and, because we focus on the low QD density region of the sample, the number of holes per QD is rather important: We obtain, for instance, that two holes dwell in the QDs for $n_A \approx 10^{11}$ cm^{-3}. For larger C doping densities, the QD occupancy increases more slowly with increasing n_A, while at the same time the depletion length rapidly decreases below it maximum value. For the typical acceptor densities of the order of 10^{13}–10^{14} cm^{-3},[58] the QD is nearly populated by three holes, which is more than the two-hole occupancy considered in our work hypothesis (see Sec. IV A). However, excepting an average value of the typical acceptor densities, we do not have a precise knowledge of the C doping in the QD

vicinity. Note finally that notwithstanding for low QD and acceptor densities, the model described by Eqs. (A1)–(A3) is very crude (both dot-to-dot and interacceptor mean distances become very large), it nevertheless correctly describes the

average occupancy $p_B = n_A l_M$ in the full transfer regime (i.e., when $n_A l_M / n_{QD} < 1$), which could be anticipated from a more general standpoint (i.e., statistical distribution with charge neutrality consideration).

*Present address: LPN, CNRS, 91460 Marcoussis, France.

†Present address: EPFL, CH-1015 Lausanne, Switzerland.

‡Present address: IM2NP, CNRS, AMU, 13397 Marseille, France.

§carole.diederichs@lpa.ens.fr

[1] R. Ferreira and G. Bastard, Appl. Phys. Lett. **74**, 2818 (1999).

[2] I. Magnusdottir, A. V. Uskov, S. Bischoff, B. Tromborg, and J. Mork, J. Appl. Phys. **92**, 5982 (2002).

[3] A. V. Uskov, J. McInerney, F. Adler, H. Schweizer, and M. H. Pilkuhn, Appl. Phys. Lett. **72**, 58 (1998).

[4] I. Magnusdottir, S. Bischoff, A. V. Uskov, and J. Mork, Phys. Rev. B **67**, 205326 (2003).

[5] B. Ohnesorge, M. Albrecht, J. Oshinowo, A. Forchel, and Y. Arakawa, Phys. Rev. B **54**, 11532 (1996).

[6] D. Elvira, R. Hostein, B. Fain, L. Monniello, A. Michon, G. Beaudoin, R. Braive, I. Robert-Philip, I. Abram, I. Sagnes, and A. Beveratos, Phys. Rev. B **84**, 195302 (2011).

[7] G. A. Narvaez, G. Bester, and A. Zunger, Phys. Rev. B **74**, 075403 (2006).

[8] T. S. Sosnowski, T. B. Norris, H. Jiang, J. Singh, K. Kamath, and P. Bhattacharya, Phys. Rev. B **57**, 9423(R) (1998).

[9] T. Muller, F. F. Schrey, G. Strasser, and K. Unterrainer, Appl. Phys. Lett. **83**, 3572 (2003).

[10] L. Zhang, T. F. Boggess, K. Gundogdu, M. E. Flatté, D. G. Deppe, C. Cao, and O. B. Shchekin, Appl. Phys. Lett. **79**, 3320 (2001).

[11] J. Siegert, S. Marcinkevicius, and Q. X. Zhao, Phys. Rev. B **72**, 085316 (2005).

[12] C. Kammerer, G. Cassabois, C. Voisin, M. Perrin, C. Delalande, Ph. Roussignol, and J. M. Gérard, Appl. Phys. Lett. **81**, 2737 (2002).

[13] A. Berthelot, I. Favero, G. Cassabois, C. Voisin, C. Delalande, Ph. Roussignol, R. Ferreira, and J. M. Gérard, Nat. Phys. **2**, 759 (2006).

[14] P. Michler, A. Kiraz, C. Becher, W. V. Schoenfeld, P. M. Petroff, L. Zhang, E. Hu, and A. Imamoglu, Science **290**, 2282 (2000).

[15] C. Santori, D. Fattal, J. Vuckovic, G. S. Solomon, and Y. Yamamoto, Nature (London) **419**, 594 (2002).

[16] A. Zrenner, E. Beham, S. Stufler, F. Findeis, M. Bichler, and G. Abstreiter, Nature (London) **418**, 612 (2002).

[17] J. P. Reithmaier, G. Sek, A. Loffler, C. Hofmann, S. Kuhn, S. Reitzenstein, L. V. Keldysh, V. D. Kulakovskii, T. L. Reinecke, and A. Forchel, Nature (London) **432**, 197 (2004).

[18] T. Yoshie, A. Scherer, J. Hendrickson, G. Khitrova, H. M. Gibbs, G. Rupper, C. Ell, O. B. Shchekin, and D. G. Deppe, Nature (London) **432**, 200 (2004).

[19] C. Kammerer, C. Voisin, G. Cassabois, C. Delalande, Ph. Roussignol, F. Klopf, J. P. Reithmaier, A. Forchel, and J. M. Gérard, Phys. Rev. B **66**, 041306 (2002).

[20] A. Muller, E. B. Flagg, P. Bianucci, X. Y. Wang, D. G. Deppe, W. Ma, J. Zhang, G. J. Salamo, M. Xiao, and C. K. Shih, Phys. Rev. Lett. **99**, 187402 (2007).

[21] R. Melet, V. Voliotis, A. Enderlin, D. Roditchev, X. L. Wang, T. Guillet, and R. Grousson, Phys. Rev. B **78**, 073301 (2008).

[22] S. Ates, S. M. Ulrich, S. Reitzenstein, A. Loffler, A. Forchel, and P. Michler, Phys. Rev. Lett. **103**, 167402 (2009).

[23] A. N. Vamivakas, Y. Zhao, C. Y. Lu, and M. Atature, Nat. Phys. **5**, 198 (2009).

[24] H. S. Nguyen, G. Sallen, C. Voisin, Ph. Roussignol, C. Diederichs, and G. Cassabois, Phys. Rev. Lett. **108**, 057401 (2012).

[25] A. Reinhard, T. Volz, M. Winger, A. Badolato, K. J. Hennessy, E. L. Hu, and A. Imamoglu, Nat. Phot. **6**, 93 (2012).

[26] H. S. Nguyen, G. Sallen, C. Voisin, Ph. Roussignol, C. Diederichs, and G. Cassabois, Appl. Phys. Lett. **99**, 261904 (2011).

[27] C. Matthiesen, A. N. Vamivakas, and M. Atature, Phys. Rev. Lett. **108**, 093602 (2012).

[28] K. Konthasinghe, J. Walker, M. Peiris, C. K. Shih, Y. Yu, M. F. Li, J. F. He, L. J. Wang, H. Q. Ni, Z. C. Niu, and A. Muller, Phys. Rev. B **85**, 235315 (2012).

[29] T. Volz, A. Reinhard, M. Winger, A. Badolato, K. J. Hennessy, E. L. Hu, and A. Imamoglu, Nat. Phot. **6**, 605 (2012).

[30] J. Houel, A. V. Kuhlmann, L. Greuter, F. Xue, M. Poggio, B. D. Gerardot, P. A. Dalgarno, A. Badolato, P. M. Petroff, A. Ludwig, D. Reuter, A. D. Wieck, and R. J. Warburton, Phys. Rev. Lett. **108**, 107401 (2012).

[31] O. Gazzano, S. Michaelis de Vasconcellos, C. Arnold, A. Nowak, E. Galopin, I. Sagnes, L. Lanco, A. Lemaitre, and P. Senellart, Nat. Com. **4**, 1425 (2013).

[32] M. Hayne, O. Razinkova, S. Bersier, R. Heitz, L. Muller-Kirsch, M. Geller, D. Bimberg, and V. V. Moshchalkov, Phys. Rev. B **70**, 081302(R) (2004).

[33] D. V. Regelman, E. Dekel, D. Gershoni, E. Ehrenfreund, A. J. Williamson, J. Shumway, A. Zunger, W. V. Schoenfeld, and P. M. Petroff, Phys. Rev. B **64**, 165301 (2001).

[34] M. Ediger, P. A. Dalgarno, J. M. Smith, B. D. Gerardot, R. J. Warburton, K. Karrai, and P. M. Petroff, Appl. Phys. Lett. **86**, 211909 (2005).

[35] J. Gomis-Bresco, G. Munoz-Matutano, J. Martinez-Pastor, B. Alen, L. Seravalli, P. Frigeri, G. Trevisi, and S. Franchi, New J. Phys. **13**, 023022 (2011).

[36] M. Grundmann and D. Bimberg, Phys. Rev. B **55**, 9740 (1997).

[37] I. Pelant and J. Valenta, *Luminescence Spectroscopy of Semiconductors* (Oxford University Press, New York, 2012).

[38] G. Cassabois, C. Kammerer, R. Sopracase, C. Voisin, C. Delalande, Ph. Roussignol, and J. M. Gérard, J. Appl. Phys. **91**, 5489 (2002).

[39] S. Raymond, K. Hinzer, S. Fafard, and J. L. Merz, Phys. Rev. B **61**, 16331 (2000).

[40] G. Medeiros, D. Leonard, and P. Petroff, Appl. Phys. Lett. **66**, 1767 (1995).

[41] E. O. Göbel, J. Kuhl, and R. Hoger, J. Lumin. **30**, 541 (1985).

[42] A. Schliwa, M. Winkelnkemper, and D. Bimberg, Phys. Rev. B **79**, 075443 (2009).

[43] A. Jankovic, R. Ferreira, and G. Bastard, Physica E **21**, 252 (2004).

[44] M. Abbarchi, F. Troiani, C. Mastrandrea, G. Goldoni, T. Kuroda, T. Mano, K. Sakoda, N. Koguchi, S. Sanguinetti, A. Vinattieri, and M. Gurioli, Appl. Phys. Lett. **93**, 162101 (2008).

[45] U. Bockelmann and T. Egeler, Phys. Rev. B **46**, 15574 (1992).

[46] I. Favero, A. Berthelot, G. Cassabois, C. Voisin, C. Delalande, Ph. Roussignol, R. Ferreira, and J.-M. Gérard, Phys. Rev. B **75**, 073308 (2007).

[47] V. Zwiller, H. Blom, P. Jonsson, N. Panev, S. Jeppesen, T. Tsegaye, E. Goobar, M.-E. Pistol, L. Samuelson, and G. Bjork, Appl. Phys. Lett. **78**, 2476 (2001).

[48] Z. Yuan, B. E. Kardynal, R. M. Stevenson, A. J. Shields, C. J. Lobo, K. Cooper, N. S. Beattie, D. A. Ritchie, and M. Pepper, Science **295**, 102 (2002).

[49] G. Sallen, A. Tribu, T. Aichele, R. André, L. Besombes, C. Bougerol, M. Richard, S. Tatarenko, K. Kheng, and J.-Ph. Poizat, Nat. Phot. **4**, 696 (2010).

[50] G. Sallen, A. Tribu, T. Aichele, R. André, L. Besombes, C. Bougerol, M. Richard, S. Tatarenko, K. Kheng, and J.-Ph. Poizat, Phys. Rev. B **84**, 041405(R) (2011).

[51] H. D. Robinson and B. B. Goldberg, Phys. Rev. B **61**, 5086(R) (2000).

[52] L. Besombes, K. Kheng, L. Marsal, and H. Mariette, Phys. Rev. B **65**, 121314(R) (2002).

[53] M. Abbarchi, T. Kuroda, T. Mano, M. Gurioli, and K. Sakoda, Phys. Rev. B **86**, 115330 (2012).

[54] C. Santori, D. Fattal, J. Vuckovic, G. S. Solomon, E. Waks, and Y. Yamamoto, Phys. Rev. B **69**, 205324 (2004).

[55] B. Pietka, J. Suffczynski, M. Goryca, T. Kazimierczuk, A. Golnik, P. Kossacki, A. Wysmolek, J. A. Gaj, R. Stepniewski, and M. Potemski, Phys. Rev. B **87**, 035310 (2013).

[56] A. Högele, S. Seidl, M. Kroner, K. Karrai, R. J. Warburton, B. D. Gerardot, and P. M. Petroff, Phys. Rev. Lett. **93**, 217401 (2004).

[57] J.-N. Isaia, L.-A. de Vaulchier, S. Hameau, R. Ferreira, Y. Guldner, E. Deleporte, J. Zeman, V. Thierry-Mieg, and J.-M. Gérard, Eur. Phys. J. B **35**, 209 (2003).

[58] E. S. Moskalenko, V. Donchev, K. F. Karlsson, P. O. Holtz, B. Monemar, W. V. Schoenfeld, J. M. Garcia, and P. M. Petroff, Phys. Rev. B **68**, 155317 (2003).